SiC–CNT nanocomposites: high pressure reaction synthesis and characterization

2006 J. Phys.: Condens. Matter 18 275

(http://iopscience.iop.org/0953-8984/18/1/020)

INSTITUTE OF PHYSICS PUBLISHING JOURNAL OF PHYSICS: CONDENSED MATTER

J. Phys.: Condens. Matter **18** (2006) 275–282 doi:10.1088/0953-8984/18/1/020

SiC–CNT nanocomposites: high pressure reaction synthesis and characterization

Y Wang[1], G A Voronin[1], T W Zerda[1,3] and A Winiarski[2]

[1] Department of Physics and Astronomy, Texas Christian University, Fort Worth, TX 76129, USA
[2] A Chelkowski Institute of Physics, Silesian University, 40-007 Katowice, Poland

E-mail: t.zerda@tcu.edu

Received 27 June 2005
Published 9 December 2005
Online at stacks.iop.org/JPhysCM/18/275

Abstract

Silicon carbide–carbon nanotube composite was fabricated using the high pressure reactive sintering technique. Samples were synthesized at high pressures, 2 and 8 GPa, and temperatures, 1770 and 1970 K. Their structures were studied using x-ray diffraction, x-ray photoelectron spectroscopy, transmission electron microscopy, and Raman scattering techniques. The composites produced at high pressure have pronounced nanocrystalline structure (the mean crystallite size of the SiC matrix was 32–37 nm) and very promising mechanical properties: fracture toughness of 6.8–7.1 MPa $m^{0.5}$ and Vickers hardness of 20–21 GPa.

1. Introduction

Carbon nanotubes (CNT) have been a subject of extensive research because of their exceptional mechanical and physical properties. Due to these properties, CNT have great potential for a variety of applications [1–3]. One of most promising among them is composite reinforcement. Most of the works in this field are devoted to processing and characterization of polymer–CNT and metal–CNT composites [4–10], while research on the development of ceramic–CNT composites is limited [11–15]. In most cases, ceramic–CNT composites were sintered by a conventional hot isostatic press sintering method and have shown only a slight enhancement, or even a deterioration, of the mechanical properties. The main reason for such modest progress in the development of CNT-reinforced ceramics is most probably the absence of substantial adhesion between the ceramic matrix and the slick sp^2 plane of the nanotube, which prevents taking full advantage of the great strength of carbon nanotubes. In this work we report results on SiC–CNT nanocomposite synthesis by the high pressure reaction sintering technique and discuss their structure and mechanical properties. The reaction sintering technique allows alleviation of some of the above-mentioned problems and may be a promising method for processing ceramic–CNT composites with advanced mechanical properties.

[3] Author to whom any correspondence should be addressed.

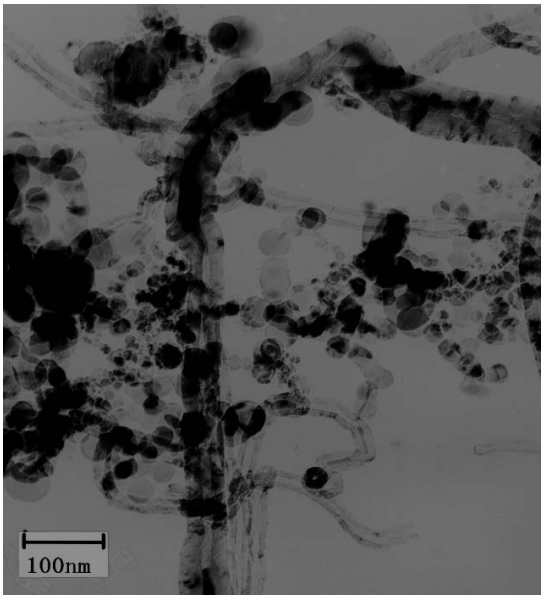

Figure 1. Typical TEM image of the initial silicon–MWNT mixture.

2. Experimental details

Silicon nanopowder of particle size 30–50 nm and purity 98+% and multiwall carbon nanotubes (MWNT) of purity 95+% and outside diameters between 60 and 100 nm, from Nanostructured & Amorphous Materials, Inc., were used in this study. The lengths of the MWNT varied, but in most cases they were several micrometres long.

Homogeneous mixtures of Si nanocrystals and multiwall nanotubes in weight proportion 3:2 were made by high energy sonication in ethanol for 30 min and subsequent drying in argon at temperature 400 K. Transmission electron microscope (TEM) images showed that silicon particles were fairly homogeneously dispersed around nanotubes, although some small Si agglomerates and nanotube bundles were observed (figure 1).

Composite samples were made by the high pressure sintering technique [16]. Sintering experiments at 2 GPa were run in a cylinder cell equipped with a tight-fitting piston. Experiments at the higher pressure, 8 GPa, were run in a toroidal cell that consisted of two identical anvils with toroidal grooves and a lithographic stone gasket that matched the contours of the grooves [17]. Si–MWNT mixtures were packed inside a cylindrical graphite heater placed inside the cylinder (2 GPa) or in the hole in the centre of a gasket (8 GPa).

Pressure calibration of the toroidal cell was carried out by recording phase transitions of Bi and PbTe. Temperature calibration was carried out by measuring the temperature in the centre of the high pressure cell using a $W_{3\%}Re/W_{25\%}Re$ thermocouple, as a function of the electric power dissipated in the apparatus. The power–temperature and load–pressure plots obtained were used as the calibration curves for subsequent HPHT sintering. The precisions of the pressure and temperature measurements were 0.2 GPa and 50 K, respectively. In the case of the cylinder–piston cell, pressure was measured directly by a pressure gauge with precision of about 0.1 GPa and temperature by a thermocouple placed inside the specimen with accuracy better than 25 K.

The experiments were run according to the following protocol. The pressure was raised to the terminal value at room temperature. Next, temperature was increased to 1770 K or

Table 1. SiC phase structural parameters, hardness, and fracture toughness of SiC–MWNT composites sintered at the pressure 8 GPa and different temperatures.

Sintering temperature (K)	SiC structural parameters		Vickers hardness H_V (GPa) ($P = 4.9$ N)	Fracture toughness K_{IC}, (MPa m$^{0.5}$)
	$\langle x \rangle_{vol}$ (nm)	ε (%)		
1770	37 ± 5	0.4	21 ± 2	7.1 ± 0.9
1970	34 ± 6	0.4	20 ± 2	6.8 ± 0.8

1970 K at a rate of 200 K s^{-1}, and the samples were kept at that temperature for 30 s. Finally, temperature was decreased to room level and the pressure released.

The sintered samples were ground to form tablets of diameter 7 mm and height 2.5 mm. Both bases of the tablets were polished using diamond powders and sprays with particle sizes decreasing gradually from 5 to 0.5 μm. Three different samples of each material were prepared and the results listed in this paper are the average data obtained for these specimens.

TEM, x-ray diffraction (XRD), x-ray photoelectron spectroscopy (XPS), scanning electron microscopy (SEM), and Raman spectroscopy were used to characterize the structure of the initial Si–CNT mixtures and sintered specimens. TEM images were taken on a Philips EM300 operated at 60 kV. X-ray diffraction patterns were measured with a PW Philips diffractometer with Cu Kα radiation ($\lambda = 1.540\,56$ Å), operated at 35 kV and 30 mA. The measurement range of 2Θ was from 20° to 150° with a step of 0.02° and an exposure time of 3 s. XPS spectra were recorded using the multitechnique electron spectrometer PHI 5700/660 from Physical Electronics. The x-ray tube was operated at 15 kV and 17 mA. A quartz monochromator was used to separate Al Kα x-ray radiation, which was focused on the sample. Photoelectrons were collected from the area with the diameter of 0.8 mm using a multichannel detector. The XPS spectra were analysed using a Multipak program from Physical Electronics. An SEM microscope, JEOL SM-6100, was used to examine the surfaces of the sintered specimens. The probe current ranged from 10^{-12} to 10^{-6} A and magnifications ranging from 750 to 3000 were used. Raman scattering spectra were obtained at room temperature using a homemade Raman microimaging system. Two lasers operating at 780 and 514 nm wavelengths were used to study Raman scattering.

The Vickers microindentation hardness was measured using a Buehler Micromet 2003 tester; the load applied to the indenter was 4.9 N. The fracture toughness stress intensity factor K_{IC} was measured using a Buehler Macromet tester by the indentation method [18] with a load 147 N using a Vickers diamond indenter.

3. Results

X-ray diffraction patterns of the initial Si–MWNT mixture and selected composites are shown in figure 2. The x-ray diffraction peaks of SiC demonstrate significant line broadening, comparable to that of the initial silicon powder. X-ray diffraction patterns of composite samples sintered at 8 GPa have been refined with General Structure Analysis Software (GSAS) [19]. Individual peaks were fitted with a pseudo-Voigt function. The volume-averaged crystallite size and microstrains were estimated using the Warren–Averbach approach. The results of the GSAS analysis are listed in table 1.

XPS scans reveal the presence of carbon, silicon, and oxygen. The carbon C 1s peak clearly has two components, one at 284.4 eV and another at 283.5 eV; figure 3. These binding

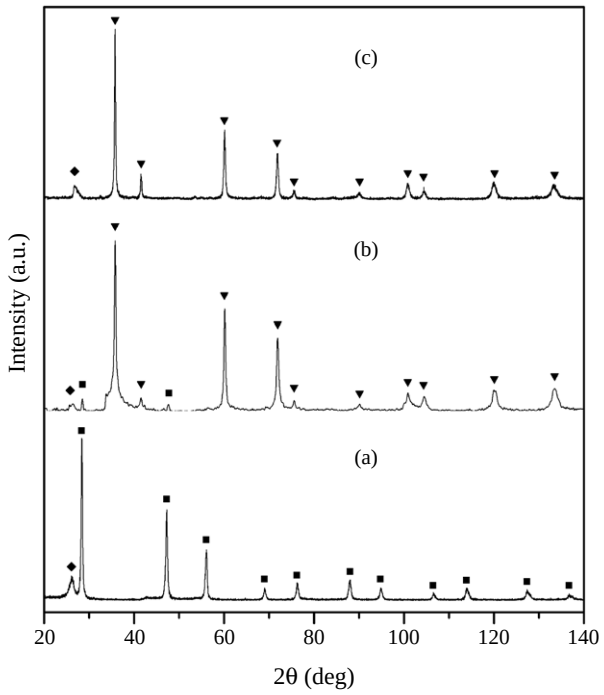

Figure 2. XRD of the initial Si–MWNT mixture (a), and SiC–CNT samples sintered at $T = 1770$ K and 2 GPa (b) and 8 GPa (c). Squares—reflections due to silicon; diamond—CNT.

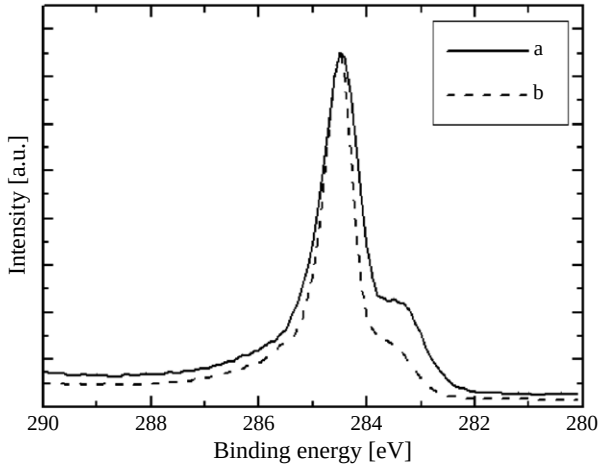

Figure 3. XPS spectra of composites sintered at 1770 K and 2 GPa, broken line, and 8 GPa, solid line. C 1s region.

energies are indicative of graphite-like systems and SiC, respectively [20]. From figure 3 it is seen that the relative intensity of the SiC peak increased with pressure. Samples prepared in the low pressure region, see figure 4, have a silicon Si 2p peak composed of two bands, one centred at about 101.3 eV (due to SiC) and another at 103.5 eV (8 GPa) or 104.7 (2 GPa) eV (identified as due to SiO_2). At certain locations on the surface of the specimen sintered at

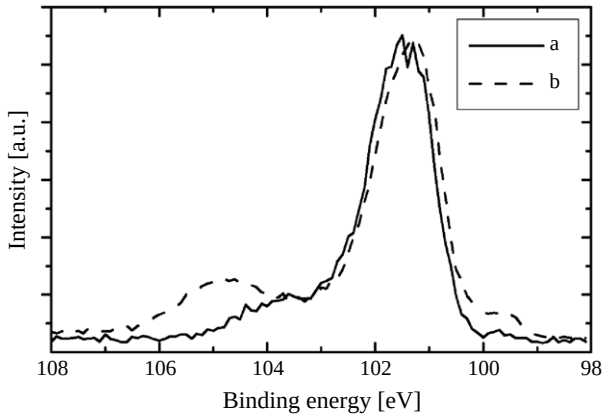

Figure 4. XPS spectra of composites sintered at 1770 K and 2 GPa, broken line, and 8 GPa, solid line. Si 2p region.

2 GPa there was also a small peak at about 99 eV due to crystalline silicon [20]. In the spectra obtained for the specimens sintered at 8 GPa, the SiC peak was strong and the other two components were negligibly small. The oxygen O 1s peaks were detected for all composites and had similar binding energies and band shapes; they are not shown here. It is worth noticing that the intensities of the oxygen peaks were small for the 8 GPa specimens.

For the XPS measurements all samples were placed inside the vacuum chamber and mechanically broken under ultrahigh vacuum conditions into two segments; the freshly uncovered surfaces were never exposed to the atmosphere. To ensure that observed spectra are due to atoms chemically bonded to the composite and not ones physically adsorbed by the surface, spectra were recorded before and after the specimens were sputtered for 2 min with Ar ions with the energy of 1 keV. No changes in band positions were observed. It is very likely that the specimens broke where their structure was the weakest, probably where the concentration of silica and/or nanotubes was high. Therefore, the intensities of the bands measured by the XPS technique do not necessarily provide information on the composition of the body of the specimens, but rather are limited to the exposed surface.

The Raman spectrum of one of the specimens sintered at 8 GPa is shown in figure 5. A broad peak at 794 cm^{-1} corresponds to the transverse optic (TO) phonon mode at the Γ point of the SiC Brillouin zone [21]. This peak was broad and asymmetric. The longitudinal optic (LO) phonon peak of SiC was completely suppressed when the 780 nm excitation line was used. The LO band has its intensity dependent on the wavelength of the incident laser; this effect has been discussed in detail in our previous report [22]. Close to the resonance, when the 514 nm laser excitation line carrying an energy close to that of the band gap energy of 2.4 eV was used, the LO band appeared at about 964 cm^{-1} and had an intensity similar to that of the TO band [22]. Unlike for XPS, no traces of unreacted silicon were found in the Raman spectra for all specimens. Two strong Raman peaks at about 1558 and 1345 cm^{-1} were identified as due to MWNT.

The hardness and fracture toughness of the samples are shown in table 1. Samples sintered at 2 GPa were too soft to be measured. At 8 GPa, no substantial influence of the sintering temperature on the composite properties was observed. Differences in hardness and fracture toughness values of the samples sintered at different temperatures were within the corresponding error margins.

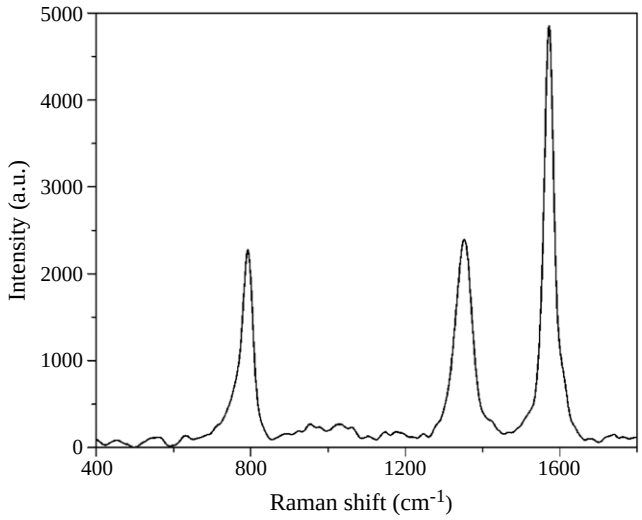

Figure 5. Raman spectrum of the SiC–MWNT sample sintered at 8 GPa and 1770 K, after background subtraction. A 780 nm laser was used as the excitation light.

4. Discussion

Assuming that all the silicon and carbon has reacted, the composites should contain 86 wt% SiC, leaving about 14% of the carbon unreacted. From XRD we found that most of the unreacted carbon was in the form of MWNT, although we cannot exclude the possibility of the presence of amorphous carbon. X-ray diffraction peaks indicate that carbon nanotubes survived high pressure treatment. This result is similar to that obtained by Munoz *et al* who synthesized SiC nanorods by placing CNT between silicon wafers and heating them up to 1000 °C [23]. Of course, the concentration of the residual carbon depended on the sintering conditions and from XPS and XRD studies it was obvious that in specimens manufactured at 2 GPa there was less SiC than in samples prepared at 8 GPa. At the present time we cannot explain the effect of pressure on the efficiency of the reaction. We have not observed a similar trend during the manufacturing of diamond–silicon carbide composites [16].

Analysis of XRD peak profiles has shown that the SiC phase of the composite has pronounced nanocrystalline structure: its volume-averaged crystallite size is in the range 32–37 nm. The large broadening of the Raman TO phonon peak (the linewidth at half-maximum is 20 cm^{-1}) may be attributed to both phonon confinement in nanocrystals and lattice imperfections [22, 24, 25].

Similar structural parameters of the SiC phase for composites sintered at 8 GPa and 1770 and 1970 K indicate the absence of noticeable recrystallization in the temperature interval studied. This observation can be explained by the recrystallization restraining role of both nanotubes [15] and high pressure. It is worth noticing that nanoceramics sintered by other methods [26] showed a pronounced recrystallization tendency.

The composites obtained at 2 GPa were soft and we could not measure their hardness or fracture toughness. Their density was about 1.20 g cm^{-3}. As seen in figure 6, the surface was porous and contained randomly distributed MWNT. Also, the presence of oxygen, mainly in the form of silica, but also in various C–O and C–O–Si bonds, further weakened the composite. However, when the reaction was conducted at 8 GPa we found that the concentration of oxygen

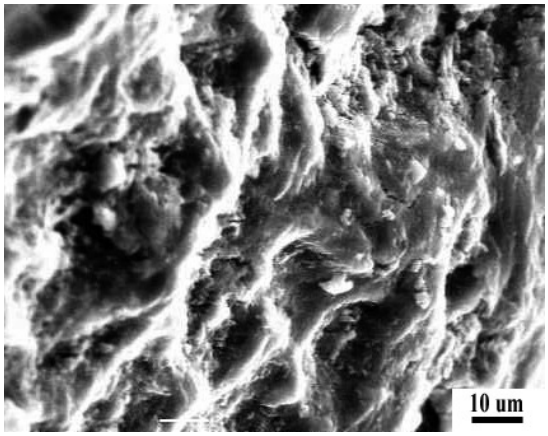

(a)

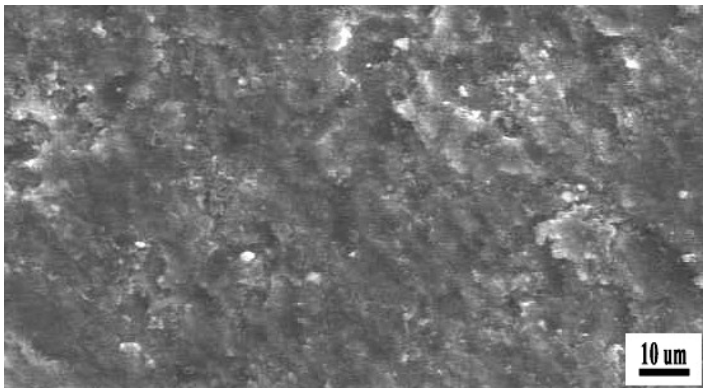

(b)

Figure 6. SEM images of ruptured surfaces of specimens obtained at 1770 K and (a) 2 GPa and (b) 8 GPa. Agglomerates of silicon carbide coated MWNT can be recognized in (a).

was much lower. In the cylinder–piston-type cell used during the low pressure sintering we employed talc as an insulating material. At high temperatures, the talc released water and oxygen, which subsequently reacted with the mixture inside the high pressure cell. The lack of oxygen in specimens obtained at 8 GPa is a result of the configuration of the toroidal cell, which did not require talc. We could not quantify the amount of oxygen from XPS intensities. XPS probes only the surface of the specimen, not its interior. Elemental analysis was also not conclusive; the specimens were very hard and difficult to completely pulverize. The high hardness of composites sintered at 8 GPa is also a result of the lack of graphite.

The density of the composite samples produced at 8 GPa, 1.40 g cm^{-3} is greater than the density of specimens obtained at 2 GPa, 1.20 g cm^{-3}, which is probably a result of the lower porosity of the samples obtained at higher pressure; compare the SEM images shown in figure 6. These samples have remarkably high fracture toughness, which may be attributed to the reinforcing properties of carbon nanotubes. The reaction between Si and CNT should proceed faster at defects of the outer shells, resulting in uneven penetration of the growing SiC crystals into the multiwall carbon nanotubes. In addition, nonuniform distribution of silicon around CNT contributed to this effect. As a result, the unreacted interior of the nanotubes, which remain in the composite, should be interlocked with the silicon carbide nanocrystalline

matrix. Such structure will provide an effective mechanism of stress transfer between the composite phases.

At the present stage of this research we cannot characterize the degree of deformation of the nanotubes in the composites after the high pressure, high temperature reaction. This topic will be the subject of future Raman studies.

Acknowledgment

This study was partially supported by the grant NSF-DMR-0502136.

References

[1] Iijima S 2002 *Physica* B **323** 1
[2] Tsukagoshi K, Yoneya N, Uryu S, Aoyagi Y, Kanda A, Ootuka Y and Alphenaar B W 2002 *Physica* B **323** 107
[3] de Heer W A 2004 *MRS Bull.* **29** 281
[4] Gong X, Liu J, Baskaran S, Voise R D and Young J S 2000 *Chem. Mater.* **12** 1049
[5] Haggenmueller R, Gommans H H, Rinzler A G, Fischer J E and Winey K I 2000 *Chem. Phys. Lett.* **330** 219
[6] Barraza H J, Pompeo F, O'Rear E A and Resasco D E 2002 *Nano Lett.* **2** 797
[7] Thostenson E T and Chou T-W 2002 *J. Phys. D: Appl. Phys.* **35** L77
[8] Velasco-Santos C, Martínez-Hernández A L, Fisher F, Ruoff R and Castaño V M 2003 *J. Phys. D: Appl. Phys.* **36** 1423
[9] Tang W, Santare M H and Advani S G 2003 *Carbon* **41** 2779
[10] Dong S R, Tu J P and Zhang X B 2001 *Mater. Sci. Eng.* C **A313** 83
[11] Ma R Z, Wu J, Wei B Q, Liang J and Wu D H 1998 *J. Mater. Sci.* **33** 5243
[12] An J-W, You D-H and Lim D-S 2003 *Wear* **255** 677
[13] Peigney A, Flahaut E, Laurent C, Chastel F and Rousset A 2002 *Chem. Phys. Lett.* **352** 20
[14] Balazsi C, Konya Z, Weber F, Biro L P and Arato P 2003 *Mater. Sci. Eng.* C **23** 1133
[15] Zhan G-D, Kuntz J D, Wan J and Mukherjee A K 2003 *Nat. Mater.* **2** 38
[16] Voronin G A, Zerda T W, Qian J, Zhao Y, He D and Dub S N 2003 *Diamond Relat. Mater.* **12/9** 1477
[17] Khvostantsev L G, Vereshchagin L F and Novikov A P 1977 *High Temp.-High Pressures* **9** 637
[18] Anatis G R, Chantkul P, Lawn B R and Marshall D W 1981 *J. Am. Ceram. Soc.* **64** 533
[19] Larson A C and Von Dreele R B 2000 General structure analysis system (GSAS) *Los Alamos National Laboratory Report LAUR 86-748*
[20] Ho G W, Wong A S W, Wee A T S and Welland M E 2004 *Nano Lett.* **4** 2023
[21] Zhang S, Zhu B, Huang F, Yan Y, Shang E, Fan S and Han W 1999 *Solid State Commun.* **111** 647
[22] Wieligor M, Wang Y and Zerda T W 2005 *J. Phys.: Condens. Matter* **17** 2387
[23] Muñoz E, Dalton A B, Collins S, Zakhidov A A, Baughman R H, Zhou W L, He J, O'Connor C J, McCarthy B and Blau W J 2002 *Chem. Phys. Lett.* **359** 397
[24] Rohmfeld S, Haundhausen M and Ley L 1998 *Phys. Rev.* B **58** 9858
[25] DiGregorio J F, Furtak T E and Petrovic J J 1992 *J. Appl. Phys.* **71** 3524
[26] Seal S, Kuiry S C, Georgieva P and Agarval A 2004 *MRS Bull.* **29** 16